Dynamical Mapping of *E. coli* Thioredoxin via ^{13}C NMR Relaxation Analysis

David M. LeMaster*,‡ and Diana M. Kushlan†

Contribution from the Department of Biochemistry and National Magnetic Resonance Facility at Madison, University of Wisconsin−Madison, 420 Henry Mall, Madison, Wisconsin 53706, and College of Veterinary Medicine, University of Illinois, 2001 S. Lincoln Ave., Urbana, Illinois 61801

Received March 18, 1996[⊗]

Abstract: NMR relaxation analysis was used to characterize the internal dynamics of oxidized *E. coli* thioredoxin in both the picosecond-nanosecond and microsecond-millisecond frequency ranges for 413 H−C and H−N bond vectors. The ^{13}C relaxation data was obtained utilizing protein samples possessing an alternating $^{13}C-^{12}C-^{13}C$... labeling pattern for most enriched sites. When combined with partial deuteration, this labeling pattern provides for isolated $^{1}H-^{13}C$ IS spin pairs exhibiting dynamically interpretable relaxation behavior. Side chains were found to exhibit a far broader range of dynamics than have been previously characterized for main chain resonances. The dynamics of structurally buried aromatic and leucine side chains are interpreted in terms of correlated main chain-side chain torsional oscillations. Structural regions exhibiting millisecond dynamics were found to correlate strongly with the presence of side chain-main chain or bifurcated main chain hydrogen bonds. Nuclei around the active site disulfide that exhibit mobility in the millisecond range correspond closely to the set of nuclei whose chemical shifts are altered upon reduction. The transient conformation is interpreted in terms of enhanced reactivity due to strain at the disulfide linkage.

Introduction

Information regarding the amplitude of small scale thermal motion for the heavy atoms in a protein crystal can, in principle, be obtained from analysis of the Debye-Waller (or B-) factors derived from X-ray diffraction studies.[1] However, nuclear magnetic resonance is unique in its potential to determine for most protein atoms various components of the internal motion according to both frequency and amplitude. In recent years numerous studies have probed the dynamics of amide nitrogens via ^{1}H-detected ^{15}N relaxation analysis utilizing biosynthetically enriched protein samples.[2] Such studies are limited by the fact that amide nitrogens constitute only ∼13% of the heavy atoms and are restricted primarily to the main chain. Although the corresponding analysis of relaxation at the carbon positions clearly could greatly increase the dynamical information available, two basic technical limitations have restricted its utility to date. With a few exceptions of highly soluble small peptides and proteins (e.g.,[3−5]) sensitivity limitations have necessitated high levels of ^{13}C enrichment. However, in contrast to the ^{15}N case, high level uniform ^{13}C enrichment introduces scalar and dipolar coupling interactions between the directly bonded ^{13}C nuclei. In this case the standard relaxation pulse sequences do not yield results directly interpretable in terms of the motion of the $^{1}H-^{13}C$ vector. Although more sophisicated pulse sequences have been introduced for obtaining a subset of the standard relaxation parameters for main chain C^{α} resonances,[6,7] a general solution is still wanting.

The original ^{1}H-detected heteronuclear relaxation pulse sequences were developed for nuclei bearing a single proton. When two or three geminal protons are present, interference effects between their dipolar interactions gives rise to multiexponential relaxation of the heteroatom.[8,9] Although modified pulse sequences have been introduced for suppressing these effects for methyl groups,[10,11] no such solution is currently available for the potentially more informative methylene positions.

These two problems can be overcome by a more elaborate isotopic labeling procedure. The problem of one bond $^{13}C-^{13}C$ interactions can be surmounted by isotopic enrichment at alternating carbon sites. As illustrated in Figure 1, it is possible to obtain such a pattern at most positions by expressing the protein in a suitable strain of *Escherichia coli* on a growth medium containing either [2-^{13}C]glycerol or [1,3-$^{13}C_2$]glycerol. The problem of having more than one ^{1}H attached to each ^{13}C can be overcome by combining random fractional deuteration at a moderate level (50%) with the selective ^{13}C labeling. These two labeling protocols, in combination with spectral selection for ^{13}C atoms bearing a single ^{1}H substituent, make it possible to investigate the relaxation behavior for a simple two-spin ($^{1}H-^{13}C$) system at most carbon positions in a protein.

This approach, potentially applicable to any *E. coli* expressed protein, has been applied to an investigation of the dynamics of *E. coli* thioredoxin, the best characterized member of the

* To whom correspondence should be addressed. Phone: (608)278-8539. FAX: (608)262-3453. E-mail: lemaster@nmrfam.wisc.edu.
† University of Illinois.
‡ University of Wisconsin−Madison.
⊗ Abstract published in *Advance ACS Abstracts,* September 15, 1996.

(1) Ringe, D.; Petsko, G. A. *Prog. Biophys. Mol. Biol.* **1985**, *45*, 197−235.
(2) Wagner, G. *Curr. Opin. Struct. Biol.* **1993**, *3*, 748−754.
(3) Nirmala, N. R.; Wagner, G. *J. Am. Chem. Soc.* **1988**, *110*, 7557−7558.
(4) Palmer, A. G.; Rance, M.; Wright, P. E. *J. Am. Chem. Soc.* **1991**, *113*, 4371−4380.
(5) Mispelter, J.; Lefevre, C.; Adjadj, E.; Quiniou, E.; Favaudon, V. *J. Biomolec. NMR* **1995**, *5*, 233−244.
(6) Yamazaki, T.; Muhandiram, R.; Kay, L. E. *J. Am. Chem. Soc.* **1994**, *116*, 8266−8278.
(7) Engelke, J.; Ruterjans, H. *J. Biomolec. NMR* **1995**, *5*, 173−182.
(8) Fagerness, P. E.; Grant, D. M.; Kuhlmann, K. F.; Mayne, C. L.; Parry, R. B. *J. Chem. Phys.* **1975**, *63*, 2524−2532.
(9) Vold, R. R.; Vold, R. L. *J. Chem. Phys.* **1976**, *64*, 320−332.
(10) Palmer, A. G.; Wright, P. E.; Rance, M. *Chem. Phys. Lett.* **1991**, *185*, 41−46.
(11) Nicholson, L. K.; Kay, L. E.; Baldisseri, D. M.; Arango, J.; Young, P. E.; Bax, A.; Torchia, D. A. *Biochemistry* **1992**, *31*, 5253−5263.

S0002-7863(96)00877-3 CCC: $12.00

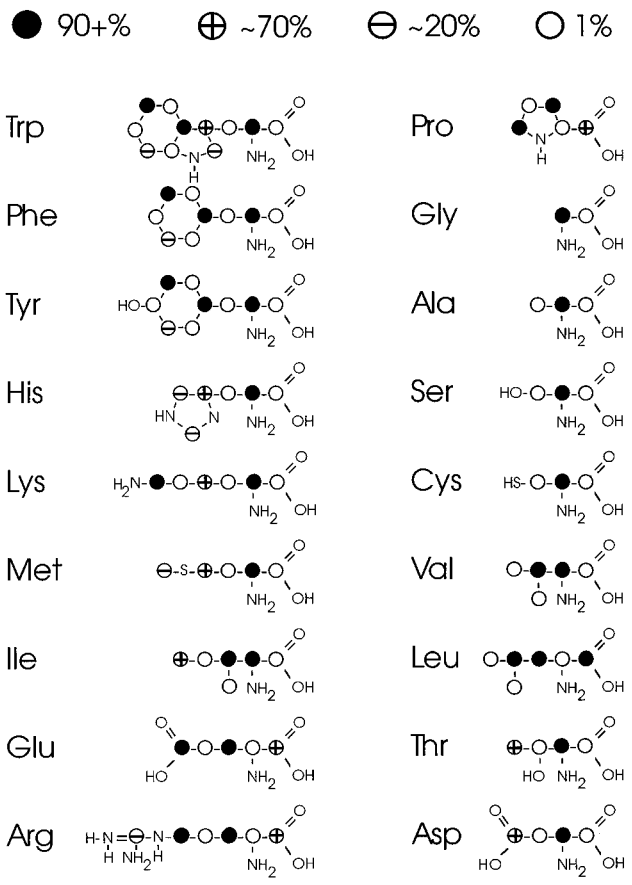

Figure 1. Alternating carbon enrichment of *E. coli* thioredoxin. Selective ^{13}C enrichment largely devoid of adjacent ^{13}C nuclei can be obtained for the various residue types via protein expression in a suitable *E. coli* strain.[77] The illustrated labeling pattern was obtained for *E. coli* thioredoxin expressed in a strain lacking succinate dehydrogenase and malate dehydrogenase grown on [2-^{13}C]glycerol and $NaH^{13}CO_3$. The opposite labeling pattern is obtained by growth on [1,3-$^{13}C_2$]glycerol with $NaH^{12}CO_3$ added to suppress recycling of decarboxylated $^{13}CO_2$. The enrichment levels were determined by acid hydrolysis, chromatographic separation of the constituent amino acids,[78] and ^{13}C NMR analysis.[77] The spectral S/N and the resolution of the ^{13}C satellite resonances were generally sufficient to allow direct verification of most of the labeling selectivity on the *E. coli* thioredoxin samples. For the proton bearing carbons only the branch sites of valine, leucine, and isoleucine exhibit high levels of adjacent ^{13}C enrichment. Modest isotope scrambling occurs for the aromatic rings due to the phosphopentose pathway exchanges. Low levels of enrichment at an adjacent aromatic position pose no significant complication as the satellite peaks from the $^{13}C-^{13}C$ coupling are well resolved from the resonance of the isolated ^{13}C nucleus.

ubiquitous thioredoxin superfamily. In bacteria and yeast thioredoxins have functions including hydrogen donation to ribonucleotide reduction and reduction of inorganic sulfate.[12,13] In eukaryotes thioredoxins regulate a host of photosynthetic enzymes,[14] activate transcription factors NF-κB, and AP-1[15,16] and recently have been shown to be identical to the adult T-cell leukemia derived factor.[17] Much of the biochemical interest in this protein stems from the fact that tandem thioredoxin modules form the active site of the mammalian protein disulfide isomerase which is essential for maturation of secreted proteins.[18]

Experimental Section

The ^{13}C enriched glycerol (Cambridge Isotopes) was deuterated to 55−60% via Raney nickel catalyzed hydrogen exchange.[19] *E. coli* strain DL323 was derived by introduction of sdh-1 (succinate dehydrogenase)[20] and mdh-2 (malate dehydrogenase)[21] into the prototrophic strain MG1655 (Coli Genetic Stock Center no. 6300). The *E. coli* thioredoxin expression plasmid pDL59[22] was transformed into DL323, and the strain was grown in M9 minimal medium containing 55% ^2H_2O. A modest average isotope selectivity gives rise to a deuteration level in the protein of ∼50%. Protein purification was carried out as described previously.[22]

Relaxation data sets were collected on a 3.5 mM sample labeled from [2-^{13}C]glycerol (denoted as [2C]-Trx) and for both a concentrated (3.0 mM) and subsequently diluted (1.5 mM) sample obtained from a [1,3-$^{13}C_2$]glycerol growth (denoted as $[1,3C]_c$-Trx and $[1,3C]_d$-Trx, respectively), in 50 mM sodium [1-^2H]formate pD 3.5 at 25 °C. These pH and ionic strength conditions closely mimic those of the sample crystallized from 2,4-methylpentanediol used for the high resolution X-ray structural analysis.[23] Cross correlation effects due to the $^2H-^{13}C$ dipole and ^2H quadrupole interactions were suppressed by addition of ^2H decoupling[24−27] to standard T_1, T_2,[28] and NOE[29] relaxation experiments. As each of these relaxation experiments utilize refocused INEPT transfers, tuning of the refocusing delay provides for efficient suppression of the I_2S signals from carbons bearing two protons.[30] Due to the ^2H isotopic shift effect the residual signals arising from the triprotio bearing methyl carbons were well resolved from the larger corresponding monoprotio methyl resonances. For the T_2 pulse sequence the order of the evolution and relaxation intervals were reversed to provide better suppression of the signal from diprotio bearing carbons.[31] Owing to the limited bandwidth of the CPMG sequence, the aliphatic spectral region was subdivided into two (3800 Hz, center = 59.4 ppm; 4438 Hz, center = 28.3 ppm) and three (3528 Hz, center = 53.3 ppm; 3700 Hz, center = 33.2 ppm; 2165 Hz, center = 14.8 ppm) frequency ranges for the T_2 measurements on the [1,3C]-Trx and [2C]-Trx samples, respectively. All reported relaxation decays exhibited apparent single exponential behavior in marked contrast to the T_2 decay patterns observed for the branch sites of valine, leucine, and isoleucine which exhibited strong modulation due to the adjacent ^{13}C nucleus. The effects of the small two bond ^{13}C homonuclear couplings present for many of the resonances appeared negligible as indicated by the absence of a systematic bias in the C^α T_2 values of amino acid residues differing in the presence of C^γ enrichment.

Noise levels were estimated from baseplane variations for the T_1 and T_2 experiments. The methine, methylene, and methyl T_1 resonances

(12) Laurent, T. C.; Moore, E. C.; Reichard, P. *J. Biol. Chem.* **1964**, *239*, 3436−3444.
(13) Black, S.; Harte, E. M.; Hudson, B.; Wartofsky, L. *J. Biol. Chem.* **1960**, *235*, 2910−2916.
(14) Wolosiuk, R.; Buchanan, B.; Crawford, N. *FEBS Lett.* **1977**, *81*, 253−258.
(15) Matthews, J.; Wakasugi, N.; Virelizier, J.; Yodoi, J.; Hay, R. *Nucleic Acids Res.* **1992**, *20*, 3821−3830.
(16) Schenk, H.; Klein, M.; Erdbrugger, W.; Droge, W.; Schulze-Ostoff, K. *Proc. Natl. Acad. Sci. U.S.A.* **1994**, *91*, 1672−1676.
(17) Tagaya, Y.; Maeda, Y.; Mitsui, A.; Kondo, N.; Matsui, M.; Hamuro, J.; Brown, N.; Arai, K.-I.; Yokota, T.; Wakasugi, H.; Yodoi, J. *EMBO J.* **1989**, *8*, 757−764.
(18) Edman, J. C.; Ellis, L.; Blacher, R. W.; Roth, R. A.; Rotter, W. J. *Nature* **1985**, *317*, 267−270.
(19) Koch, H. J.; Stuart, R. S. *Carbohyd. Res.* **1977**, *59*, C1−C6.
(20) Creaghan, I. T.; Guest, J. R. *J. Gen. Microbiol.* **1972**, *71*, 207−220.
(21) Courtright, J. B.; Henning, U. *J. Bacteriol.* **1970**, *102*, 722−728.
(22) LeMaster, D. M.; Richards, F. M. *Biochemistry* **1988**, *27*, 142−150.
(23) Katti, S.; LeMaster, D. M.; Eklund, H. *J. Mol. Biol.* **1990**, *212*, 167−184.
(24) Werbelow, L. G.; Grant, D. M. *Adv. Magn. Reson.* **1977**, *9*, 189−299.
(25) Vold, R. L.; Vold, R. R. *Prog. NMR Spectrosc.* **1978**, *12*, 79−133.
(26) London, R. E.; LeMaster, D. M.; Werbelow, L. G. *J. Am. Chem. Soc.* **1994**, *116*, 8400−8401.
(27) Grzesiek, S.; Bax, A. *J. Am. Chem. Soc.* **1994**, *116*, 10196−10201.
(28) Kay, L. E.; Nicholson, L. K.; Delaglio, F.; Bax, A.; Torchia, D. A. *J. Magn. Reson.* **1992**, *97*, 359−375.
(29) Barbato, G.; Ikura, M.; Kay, L. E.; Pastor, R. W.; Bax, A. *Biochemistry* **1992**, *31*, 5269−5278.
(30) Kushlan, D. M.; LeMaster, D. M. *J. Biomolec. NMR* **1993**, *3*, 701−708.
(31) Kushlan, D. M.; LeMaster, D. M. *J. Am. Chem. Soc.* **1993**, *115*, 11026−11027.

exhibited median experimental percent uncertainties of (3.1,3.5,1.3), (4.2,4.6,1.8), and (2.6,3.0,1.3(Thr C^{γ})+3.8(Ile C^{δ})) for the $[1,3C]_d$-Trx, $[1,3C]_c$-Trx, and [2C]-Trx samples, respectively. The corresponding median percent experimental uncertainties for the T_2 values were (2.5,4.1,4.2), (2.5,3.5,2.6), and (2.3,3.3,1.8(Thr C^{γ})+4.2(Ile C^{δ})). Noise levels in the NOE experiments were determined from the variation in peak heights for duplicate observations. The corresponding median experimental uncertainties for the NOE values were (0.033,0.035,0.022), (0.036,0.036,0.013), and (0.045,0.027,0.015).

Relaxation decay rates and their associated uncertainties were analyzed by means of Levenberg−Marquardt parameter analysis and Monte Carlo simulations[4] (software kindly provided by A. Palmer). Using a previously described protocol for assignment of the statistically minimal dynamical model,[32] molecular correlation times were determined as the value yielding the maximal number of main chain resonances fitted to the basic S^2 dynamical formalism. Reflecting the previously noted concentration dependence of the relaxation for this protein at low pH,[31] isotropic τ_c values of 7.4, 8.3, and 8.8 ns were obtained for the $[1,3C]_d$-Trx, $[1,3C]_c$-Trx, and [2C]-Trx samples, respectively.

Chemical shift anisotropy values used were -0.25×10^{-4} (aliphatic), -1.2×10^{-4} (histidine ring and tryptophan δ_1), and -1.7×10^{-4} (other aromatic carbons).[33−35] For the methylene and methyl positions the $^2H-^{13}C$ dipolar interactions are not negligible[31] and were included by assuming the same autocorrelation behavior as the geminal $^1H-^{13}C$ dipole. WALTZ[36] ^2H decoupling was applied during the ^{13}C relaxation delay and evolution using 100 μs for the nominal 90° pulse. Since ^2H decoupling cannot fully collapse the line broadening due to the dynamic frequency shift arising from the interference between the ^2H-^{13}C dipolar and ^2H quadrupolar interactions,[26,27] the $J(0)$ component was scaled to approximate this effect. In addition the finite ^2H decoupling field strength yields an estimated residual line broadening of ∼0.2 Hz per deuteron due to scalar relaxation of the second kind.[37] As with previous relaxation studies[38] a $^1H-^{13}C$ bond length of 1.07 Å was assumed. Justification for this foreshortened dipole vector has come from model calculations on both vibrational averaging[39] and on longer range $^1H-^{13}C$ dipole interactions for C^{α} [40] and monoprotio methyl resonances.[41]

The constancy of the majority of ^{15}N T_1 and T_2 values is strongly suggestive of isotropic tumbling.[42] In addition anisotropy in either the internal motions or in the overall molecular tumbling can be manifested as differential relaxation for the two geminal methylene H−C vectors. Note that the rotation of the local dihedral angles cannot cause differential relaxation due to the individual geminal H−C dipoles. The distribution of the pairwise differences in S^2 values for all the resolved nonequivalent methylene pairs in the $[1,3C]_d$-Trx sample is consistent with that drawn from a population of dynamically equivalent pairs having an rmsd of 0.043. This deviation is within that expected from the estimated median experimental uncertainties for the T_1, T_2, and NOE values of 3.5%, 4.1%, and 0.035%, respectively. Furthermore, the maximum pairwise difference corresponds to only 2.44 σ, and in no case were large pairwise differences in S^2 for the dilute sample corroborated by the data from the concentrated sample. Hence at this level of experimental accuracy there appears to be no evidence of appreciable anisotropy in either the global or local motion.

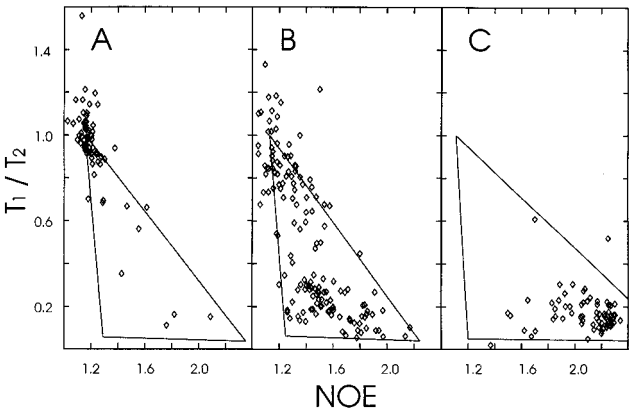

Figure 2. Distribution of the ^{13}C T_1/T_2 and NOE values for the methine, methylene and methyl resonances of *E. coli* thioredoxin. Experimental relaxation values from the $[1,3C]_d$-Trx and [2C]-Trx samples are plotted in panels A and B for the main chain methine and side chain methylene carbons, respectively. For the methyl resonances plotted in panel C the T_1/T_2 data are from the $[1,3C]_c$-Trx and [2C]-Trx samples. Both T_1/T_2 and NOE correspond to ratios of spectral density components and hence are independent of the fast limit order parameter (Eq. 1 and 2). Therefore, the mapping between (T_1/T_2, NOE) and either (S_s^2,τ_s) or (S_H^2,S_C^2) characterizes the internal motion having frequencies between the fast (ps) limit and the molecular tumbling rate. The apex of the triangles corresponds to the relaxation values predicted for rigid molecular tumbling. The triangles define the limits of relaxation values which can be exactly represented by the (S_H^2,S_C^2) (panels A and B) and (S_s^2,τ_s) (panel C) dynamical parameters. The T_1/T_2 values are normalized to the rigid isotropic tumbling limits of 30.31 and 27.58 for the methine and methylene resonances of the $[1,3C]_d$-Trx sample as well as to 42.83 and 38.81 for the [2C]-Trx sample. The lower rigid T_1/T_2 values predicted for the methylene positions represent the relaxation contributions of the attached ^2H nucleus. The methyl resonances from the $[1,3C]_c$-Trx and [2C]-Trx samples are normalized to 31.75 and 35.97, respectively.

Results

Dynamical Analysis. Selective ^{13}C enrichment combined with IS spin selection on the fractionally deuterated sample yields a substantial enhancement in resolution, particularly for the methylene positions.[30] Due to one bond $^{13}C-^{13}C$ couplings or overlap, reliable relaxation data were not obtained for Lys^{ϵ}, Phe^{ζ}, $Trp^{\eta 2}$, or the branch sites for the dimethyl amino acids (see Figure 1). Considering all other positions the relaxation behavior of over 90% of the proton bearing carbons was characterized. In Figure 2 is plotted the experimental T_1/T_2 (normalized to the that of the rigid H−C vector for isotropic molecular tumbling) and NOE values for the main chain methine (panel A), side chain methylene (panel B), and methyl resonances (panel C) of oxidized *E. coli* thioredoxin. Both the angular extent and effective time constant for the ∼nanosecond modes of motion can be qualitatively interpreted from these figures. In each panel the apex of the inscribed triangle represents the rigid limit for the isotropically tumbling H−C vector. Within the triangles the distance between the apex and the observed relaxation values is directly related to the order parameter for ∼nanosecond internal mobility, while the corresponding effective time constant decreases in a counterclockwise fashion.[32] In panel A the large majority of C^{α} resonances are clustered around the rigid limit values, indicating restricted mobility for most of the backbone. The four lowest T_1/T_2 values correspond to the first two and last two residues of the protein. In contrast, the population of side chain methylenes (panel B) exhibits a far wider range of dynamics. The low T_1/T_2 values for the methyl resonances of panel C are indicative of the angular averaging due to methyl rotation.

(32) LeMaster, D. M. *J. Biomolec. NMR* **1995**, *6*, 366−374.
(33) Prado, F. R.; Giessner-Prettre, C. *J. Magn. Reson.* **1982**, *47*, 103−117.
(34) Separovic, F.; Hayamizu, K.; Smith, R.; Cornell, B. A. *Chem. Phys. Lett.* **1991**, *181*, 157−162.
(35) Veeman, W. S. *Prog. NMR Spectroscopy* **1984**, *16*, 193−235.
(36) Shaka, A.; Keeler, J.; Freeman, R. *J. Magn. Reson.* **1983**, *53*, 313−340.
(37) Shoup, R. R.; VanderHart, D. L. *J. Am. Chem. Soc.* **1971**, *93*, 2053−2054.
(38) Palmer, A. G.; Hochstrasser, R. A.; Millar, D. P.; Rance, M.; Wright, P. E. *J. Am. Chem. Soc.* **1993**, *115*, 6333−6345.
(39) McCain, D. C.; Ulrich, E. L.; Markley, J. L. *J. Magn. Reson.* **1988**, *80*, 296−305.
(40) Allard, P.; Jarvet, J.; Ehrenberg, A.; Graslund, A. *J. Biomolec. NMR* **1995**, *5*, 133−146.
(41) Muhandiram, D. R.; Yamazaki, T.; Sykes, B. D.; Kay, L. E. *J. Am. Chem. Soc.* **1995**, *117*, 11536−11544.
(42) Stone, M. J.; Chandrasekhar, K.; Holmgren, A.; Wright, P. E.; Dyson, H. J. *Biochemistry* **1993**, *32*, 426−435.

T_1, T_2, and heteronuclear NOE relaxation due to dipolar and chemical shift anisotropy interactions arise from motional fluctuations that are characterized as a linear combination of contributions from the spectral density function $J(\omega)$ sampled at the frequencies $\omega_H+\omega_C$, ω_H, $\omega_H-\omega_C$, ω_C and 0 according to standard formulas,[43] where $\omega_H = 2\pi \times 600.1$ MHz and $\omega_C = 2\pi \times 150.9$ MHz at 14.1 T. Furthermore, conformational transitions in the microsecond−millisecond range give rise to chemical exchange line broadening which manifests itself as a reduction of the T_2 value and a corresponding increase in the apparent $J(0)$ value. Hence in general the three standard experimental relaxation values arise from six distinct dynamical parameters. One approach to circumventing this underdetermination is to measure additional independent relaxation processes so as to provide a unique correspondence to the dynamical parameters.[44] Unfortunately this spectral density mapping formalism suffers from the limitation that in practice the additional relaxation measurements do not provide dynamical information of the quality provided by the standard T_1, T_2, and NOE experiments.[45,46] A partial solution to this problem is provided by the reduced spectral density analysis[47−49] in which the standard relaxation formulas are written in terms of an average $J(\omega_{H'})$ to represent the $J(\omega_H+\omega_N)$, $J(\omega_H)$, and $J(\omega_H-\omega_N)$ terms. The chemical exchange broadening term can then be determined by measuring the field dependence of T_2 relaxation[50] or from $T_{1\rho}$ measurements for cases in which the exchange rate is approximately equal to the available spin lock field strength.[51]

An alternate approach to dynamical analysis utilizes the "model-free" formalism[52] which assumes the spectral density function arises from independent exponentially decaying correlation functions characterizing the internal motion and the overall molecular tumbling. The original formalism has been subsequently extended to represent the internal motion in terms of a fast limit order parameter and a slower motional order parameter along with the corresponding time constant[53]

$$J(\omega_i) = 2/5[S_f^2 S_s^2 \tau_m/(1 + (\omega_i\tau_m)^2) + S_f^2(1 - S_s^2)\tau_{s'}/(1 + (\omega_i\tau_{s'})^2)] \quad (1)$$

where τ_m is the molecular correlation time. More recently we have proposed an alternative extended formalism in which the internal motion is characterized by order parameters sampled at ω_C and $\omega_H+\omega_C$ as well as a fast limit order parameter.[32]

$$J(\omega_i) = 2/5S_f^2[S_H^2 S_C^2 \tau_m/(1 + (\omega_i\tau_m)^2) + (1-S_H^2)\tau_{H'}/(1+(\omega_i\tau_{H'})^2) + S_H^2(1-S_C^2)\tau_C/(1+(\omega_i\tau_C)^2)] \quad (2)$$

where $\tau_C = 1/\omega_C$ and $\tau_{H'} = 1/(\omega_H+\omega_C)$.

In the absence of chemical exchange both the (S_f^2,S_s^2,τ_s) and (S_f^2,S_H^2,S_C^2) formalisms yield a 1−1 mapping onto the experimental T_1, T_2, and NOE values over the entire ranges of the dynamical parameters.[32] For the *E. coli* thioredoxin relaxation data considered herein the ranges of these two extended model-free formalisms are given by the triangles inscribed in Figure 2. As a result, within the assumption of an effective $J(\omega_{H'})$ to represent the high frequency spectral density terms, for relaxation data lying within these boundaries the extended model-free formalisms necessarily predict the same values for $J(\omega_{H'})$, $J(\omega_C)$, and $J(0)$ as are obtained from the reduced spectral density analysis.[32] Hence in such cases the reduced spectral analysis merely provides a subset of the dynamical analysis potentially provided by the extended model free formalisms.

The equivalence among the extended model free formalisms and the reduced spectral density analysis arises because optimization of the (S_f^2,S_s^2,τ_s) and (S_f^2,S_H^2,S_C^2) parameters operationally corresponds to determination of the optimal $J(\omega_{H'})$, $J(\omega_C)$, and $J(0)$ values. Conversely, essentially exact fitting of the relaxation data for a given atom by an extended model free formalism cannot in general serve to validate the dynamical assumptions used in the derivation of that formalism. Validation of these dynamical assumptions must come from consideration of the overall population distribution, independent theoretical predictions or additional independent experimental data (e.g., field dependence relaxation measurements). For the *E. coli* thioredoxin data the constancy of the T_1/T_2 values for the vast majority of ^{15}N[42] and ^{13}C backbone atoms is strongly indicative of isotropic molecular tumbling. Furthermore, as illustrated in panel B of Figure 2 the excellent correspondence between the distribution of side chain relaxation values and range of the (S_f^2,S_H^2,S_C^2) dynamical formalism suggests that this formalism can provide an excellent minimal representation of the internal dynamics.

Given the validity of the independence of the internal mobility and molecular tumbling (note that anisotropic tumbling can be equally well accommodated[29,32,52,54]), the model free formalisms provide for partitioning of the generally more interesting spectral density contributions arising from internal dynamics which cannot be provided from the spectral density analysis approaches. Likewise the relaxation data lying above the triangles of Figure 2 indicate T_1/T_2 values larger than can be accommodated by the predicted molecular tumbling contributions and hence are suggestive of line broadening arising from chemical exchange dynamics. Once again on the basis of single field strength T_1, T_2, and NOE data the spectral density analysis formalisms cannot provide such an explicit tentative assessment of microsecond−millisecond dynamics.

The wide range of equivalence of the spectral density predictions from the extended model free formalisms indicates that optimal choice of formalism need not be straightforward. In the cases for which independent knowledge indicates a single large dominant mode of internal mobility (e.g., rapid rotation around the methyl axis) the (S_f^2,S_s^2,τ_s) formalism offers the potential of accurately extracting the time constant of this motion. Unfortunately, particularly for lower amplitude motion occuring in the neighborhood of τ_H the dynamical predictions of the (S_f^2,S_s^2,τ_s) formalism are decidedly less robust due to the operational codependence of the dynamical parameters. In contrast the dynamical parameters of the (S_f^2,S_H^2,S_C^2) formalism provide a much more robust response to variations in the input experimental relaxation data for assessment of error propagation.[32]

By explicitly incorporating the Larmor frequency dependencies in the dynamical parameters, the (S_f^2,S_H^2,S_C^2) formalism

(43) Abragam, A. *The Principles of Nuclear Magnetism*; Oxford University Press: Oxford, England, 1961.
(44) Peng, J. W.; Wagner, G. *J. Magn. Reson.* **1992**, *98*, 308−332.
(45) Peng, J. W.; Wagner, G. *Biochemistry* **1992**, *31*, 8571−8586.
(46) Peng, J. W.; Wagner, G. *Biochemistry* **1995**, *34*, 16733−16752.
(47) Farrow, N. A.; Zhang, O.; Forman-Kay, J. D.; Kay, L. E. *Biochemistry* **1995**, *34*, 868−878.
(48) Ishima, R.; Nagayama, K. *Biochemistry* **1995**, *34*, 3162−3171.
(49) Farrow, N. A.; Zhang, O.; Szabo, A.; Torchia, D. A.; Kay, L. E. *J. Biomolec. NMR* **1995**, *6*, 153−162.
(50) Gutowsky, H. S.; Holm, C. H. *J. Chem. Phys.* **1956**, *23*, 1228−1234.
(51) Szyperski, T.; Luginbuhl, P.; Otting, G.; Guntert, P.; Wuthrich, K. *J. Biomolec. NMR* **1993**, *3*, 151−164.
(52) Lipari, G.; Szabo, A. *J. Am. Chem. Soc.* **1982**, *104*, 4546−4559.
(53) Clore, G. M.; Szabo, A.; Bax, A.; Kay, L. E.; Driscoll, P. C.; Gronenborn, A. M. *J. Am. Chem. Soc.* **1990**, *112*, 4989−4991.
(54) Tjandra, N.; Feller, S. E.; Pastor, R. W.; Bax, A. *J. Am. Chem. Soc.* **1995**, *117*, 12562−12566.

serves to maximize the sensitivity of the derived order parameters to the input relaxation data.[32] Furthermore, in similarity to the spectral density analysis formalisms, it relies upon the values of the spectral density function which are directly sampled by the relaxation experiments. Focusing attention on the internal mobility characterized by the internal spectral density components $J_i(\omega)$ [i.e., $J_i(\omega) = J(\omega) - 2/5S_f^2S_H^2S_C^2\tau_m/(1+(\omega\tau_m)^2]$, the dominant Lorentzian terms of eq 2 are evaluated at their midpoint. Hence considering only these dominant terms, the internal spectral density components are quite simply related to the corresponding order parameters.

$$J_i(\omega_{H'})\cdot\omega_{H'} \sim 1/5S_f^2(1-S_H^2) \quad \text{and}$$
$$J_i(\omega_C)\cdot\omega_C \sim 1/5\, S_f^2S_H^2(1-S_C^2) \quad (3)$$

***E. coli* Thioredoxin Dynamics in the Picosecond−Nanosecond Range.** The dynamical behavior of 413 nonequivalent H−C and H−N vectors of *E. coli* thioredoxin are summarized in Figure 3. The (S_f^2,S_H^2,S_C^2) formalism partitions the internal motion at time windows of ∼picoseconds, 200 ps, and 1 ns at 14.1 T. The color scale illustrates the distribution of order parameters throughout the protein structure as monitored at these time windows. Panels A, C, and E present the S_f^2, S_H^2, and S_C^2 order parameters for the solvent accessible[55] nuclei, while the corresponding dynamical behavior of the solvent inaccessible nuclei are summarized in panels B, D, and F, respectively. As the methyl τ_s values approximate $1/\omega_H$, the S_s^2 values are displayed in panel B. Included in Figure 3 as well are the S_f^2,S_H^2, and S_N^2 values obtained via the described dynamical formalism using the previously published experimental ^{15}N relaxation values.[42]

Although a substantial fraction of the nuclei exhibit S_f^2 values less than 0.9, considerably fewer positions show significant mobility in the nanosecond time frame, particularly at τ_C. As expected the solvent inaccessible nuclei have reduced mobility which is most notable at the lower frequencies. The methyl groups provide an exception this trend as rotation around the axis occurs in the ∼200 ps time window. On the other hand, the increased mobility of the buried methyl positions is not limited to the rotation around the symmetry axis. As discussed below, for the longer side chains there is substantial mobility of the rotation axis itself. Noteworthy in Figure 3 is the large range of dynamics exhibited by the solvent exposed side chains.

As noted in the previous ^{15}N relaxation study[42] the large majority of main chain positions exhibit limited mobility in the picosecond−nanosecond time frame. Overall, the agreement between the independently obtained ^{13}C and ^{15}N relaxation data is quite satisfactory: the median difference in the individual S_f^2 values obtained for the amide N and C$^\alpha$ resonances of the same residues is only 0.042. Compared to the rest of the main chain, lower ^{15}N order parameters are observed at three short internal segments[42] which are all located around glycyl residues: G21, G74, and G92. The increased mobility at these sites is reflected in the C$^\alpha$ relaxation as well. S^2 values of 0.84, 0.86, and 0.86 for the C$^\alpha$ resonances of E30, G33 and P34 in the active site loop confirm limited mobility in the picosecond−nanosecond frequency range for residues of this region not monitored in the ^{15}N relaxation study.

With the exception of several aromatic residues, the carbons of every side chain exhibited a gradient of decreasing order parameters according to the number of bonds removed from the backbone. This trend was exhibited by both solvent-accessible and buried side chains with the gradient being generally steeper for the solvent exposed side chains as expected. On the other hand, the ring carbons of aromatic residues F12, W28, F81, and F102 exhibited S^2 values comparable to the average main chain value as had previously been observed for the tryptophan rings by both ^{15}N [42] and ^{13}C relaxation.[56] By contrast, the C$^\beta$ positions of these aromatic residues have S^2 values 0.1−0.25 lower than those of the ring carbons.

Using Phe 12 as illustration, this pattern of order parameters is interpreted in terms of anticorrelated ("crankshaft") torsional librations of χ_2 and the main chain dihedral angles. Having a χ_1 value of −158°, the Phe 12 N−C$^\alpha$ and C$^\beta$−C$^\gamma$ vectors are approximately coplanar. Using the uniform restricted diffusion model[57] a maximal 28° oscillation of the ϕ dihedral angle predicts the observed C$^\alpha$ S^2 value of 0.82. This corresponds to a 17° (i.e., $28/\sqrt{3}$) rmsd for the torsional angle fluctuation comparable to that typically estimated via molecular simulation. When the χ_1 and χ_2 dihedral angles were searched to determine the side chain orientations yielding the minimum average shift of the aromatic ring carbons (0.59 Å), the triplets (−28°,−5°,-26°) and (28°,13°,−31°) were obtained for the correlated oscillations of ϕ, χ_1, and χ_2, respectively, as illustrated in Figure 4. For these two cooperative oscillations the average angular reorientation (relative to the observed structure[23]) of the ^{1}H−^{13}C$^\beta$ and ^{1}H−^{13}C$^\delta$ dipole vectors are 32° and 11°, respectively, predicting S^2 values of 0.76 and 0.96. These predicted S^2 values agree quite well with the observed values of 0.78 and 0.93. In contrast, due to the approximate orthogonality of the C′−C$^\alpha$ and C$^\beta$−C$^\gamma$ vectors, for fluctuations of the Phe 12 main chain ψ dihedral angle no χ_1, χ_2 rotations can comparably preserve the position of the aromatic ring. As a result it is predicted that for buried aromatic amino acids the torsional fluctuations of one of the two main chain dihedral angles will be preferentially suppressed due to the restricted mobility of the aromatic ring. (Note the rarity of the 60° χ_1 dihedral angle in which the C$^\beta$−C$^\gamma$ bond is gauche to both the N−C$^\alpha$ and C′−C$^\alpha$ bonds.)

Potentially two independent order parameter estimates can be obtained for carbons adjacent to methyl groups. The factor by which the methyl S^2 is smaller than 0.111 is standardly interpreted to represent the order parameter for the rotation axis.[11] The derived mean order parameter for the rotation axis of the various methyl-bearing side chains are as follows: alanine (0.92), valine (0.84), isoleucine C$^\gamma$ (0.75), threonine (0.64), leucine (0.59), and isoleucine C$^\delta$ (0.37). In comparison the agreement is excellent for the mean S^2 values for the adjacent carbons determined independently by relaxation measurements for alanine C$^\alpha$ (0.87), threonine C$^\beta$ (0.68), and isoleucine C$^{\gamma 2}$ (0.34). The mean and range of S_{axis}^2 values obtained for the leucine methyl rotation axes correspond closely to those previously reported for the ^{13}C relaxation study of staphylococcal nuclease[11] as well as in the ^{2}H relaxation study of the C-terminal S_H^2 domain of phospholipase C$_{\gamma 1}$.[41] In addition the later study observed the most limited mobilities for the alanine residues while for three of the four isoleucine residues the C$^\delta$ nucleus exhibited an order parameter half that of the corresponding C$^\gamma$ nucleus with average S_{axis}^2 values in agreement with those observed herein. The similarity between these independent estimates of the order parameters provide strong support for the partitioning of the methyl relaxation dynamics according to independent rotation and oscillation of the rotation axis.

The shorter polar and charged side chains exhibit a wide range of dynamical behavior. The aspartic acid β carbons fall into three distinct groups. The majority exhibit S^2 values less than

(55) Lee, B.; Richards, F. M. *J. Mol. Biol.* **1971**, *55*, 379−400.
(56) Kemple, M. D.; Yuan, P.; Nollet, K. E.; Fuchs, J. A.; Silva, N.; Prendergast, F. G. *Biophys. J.* **1994**, *66*, 2111−2126.
(57) Lipari, G.; Szabo, A. *J. Am. Chem. Soc.* **1982**, *104*, 4559−4570.

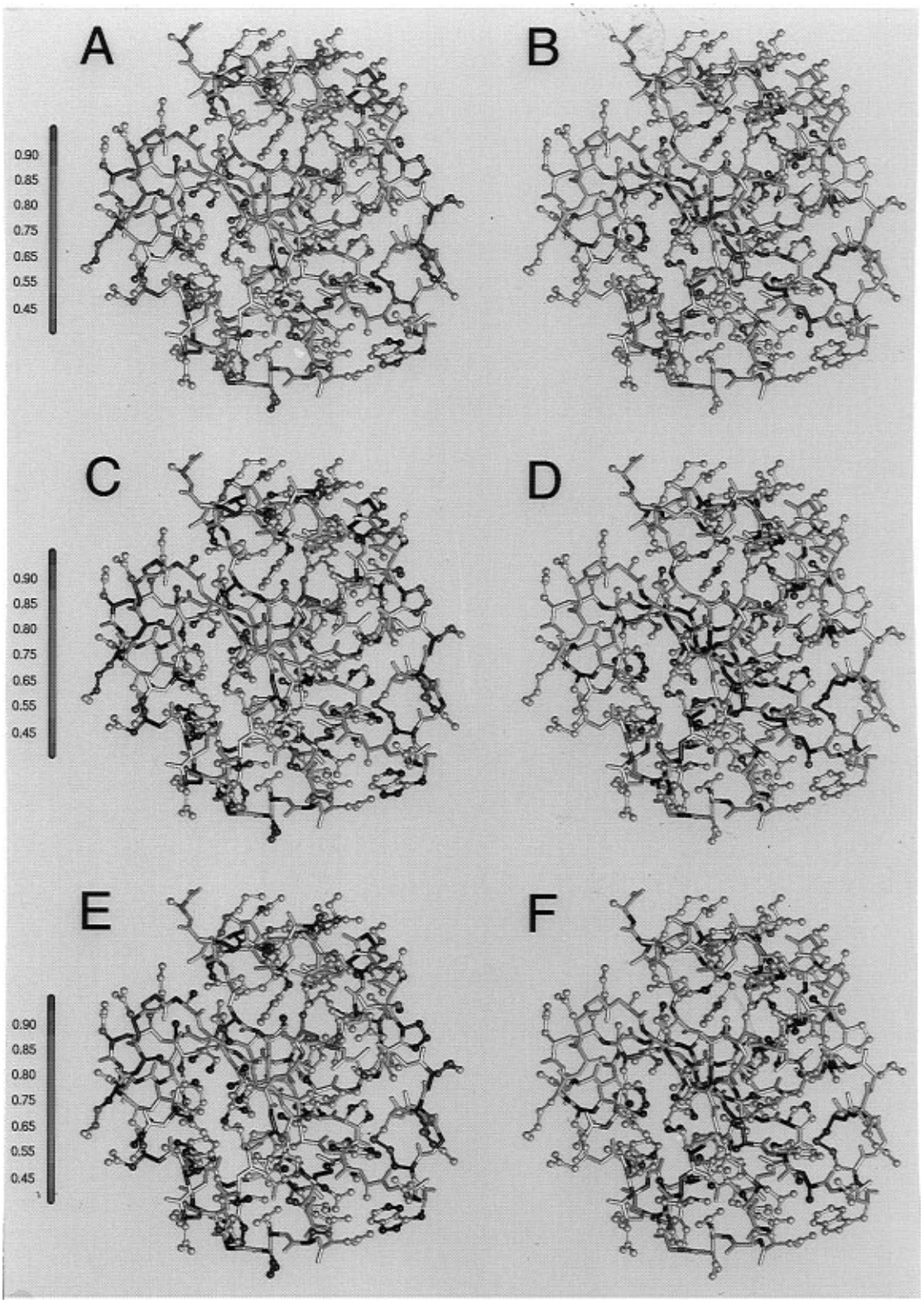

Figure 3. Order parameters from 413 independent H−C and H−N vectors of *E. coli* thioredoxin. Panels A, C, and E illustrate the S_f^2, S_H^2, and S_C^2 (or S_N^2) values obtained for solvent accessible nuclei while panels B, D, and F exhibit the corresponding order parameters for the inaccessible positions. The methyl S_s^2 values are included with S_H^2. A linear order parameter scale extending from 1.0 (blue) to 0.35 (red) is included. The color scale is graded in 0.05 steps from 1.0 to 0.75 and in 0.1 steps below. Backbone atoms are displayed with a uniform width while side chain atoms are represented as ball and stick. For visual contrast the active site disulfide is colored in pink in the lower right corner of each structure. The earlier reported ^{15}N NOE values[42] were scaled by 4.5% so as to match the average of the corresponding ^{15}N NOE values obtained at the lower pH utilized in this study. A grid search was used to obtain the optimal order parameter values (0.002 grid interval). For the (S_f^2,S_H^2,S_C^2) formalism the uncertainties in the derived order parameters closely follow the corresponding percent uncertainties in the experimental data (see legend of Figure 2) throughout the range of the formalism.[32]

0.42. D9, D15, and D104 have S^2 values clustered around 0.67. Finally, the buried D26 in the active site is highly immobilized with a S^2 value of 0.87. As seen in Tables 1 and 2 the mobility of the threonine and asparagine C$^\beta$ positions correlate completely with the presence of main chain hydrogen bonding partners as determined from the crystallographic structure.[23] This correla-

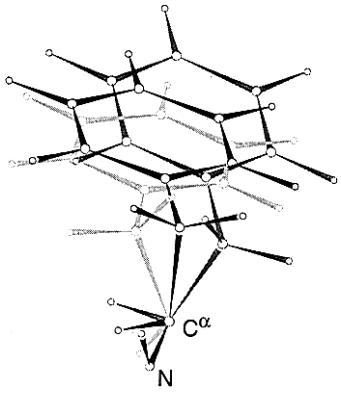

Figure 4. Model for correlated main chain-side chain torsional oscillations for Phe 12. Observed order parameters for this residue are 0.82, 0.78, and 0.93 for C^{α}, C^{β}, and C^{δ}, respectively. The increased mobility of the C^{β} relative to the ring positions can be rationalized in terms of a "crankshaft" cooperative oscillation of the main chain ϕ and side chain χ_2 dihedral angles. Illustrated are the X-ray coordinates (dark) and models for which ϕ has been varied $+/-28°$ which is the maximal angle predicted from the restricted diffusion model[57] for the C^{α} S^2 value. For all three conformations C^{α} and the preceding peptide plane are superimposed. χ_1 and χ_2 were then searched to obtain the minimal perturbation of the aromatic ring carbon positions. These model conformations [$(\chi_1,\chi_2) = (-5°,26°)$ and $(13°,-31°)$] are plotted as well. Given the variation of the H−C vectors relative to the reference X-ray structure, S^2 values of 0.76 and 0.96 are predicted for C^{β} and C^{δ}, respectively.

Table 1. Order Parameters for *E. coli* Thioredoxin Threonine Side Chains

residue	S^2 (C^{α})	S^2 (C^{β})	main chain HB partner
Thr 8	0.91	0.81	Ser 11 H^N
Thr 14	0.91	0.40	none
Thr 54	0.80	0.72	Ala 22 O (W25 mediated)
Thr 66	0.89	0.74	Asp 9 O (W74 mediated)
Thr 77	0.87	0.76	Gly 74 O

Table 2. Order Parameters for *E. coli* Thioredoxin Asparagine Side Chains

residue	S^2 (C^{α})	S^2 (C^{β})	main chain HB partner
Asn 59	0.83	0.76	Asp 61 H^N and Gln 62 H^N
Asn 63	0.88	0.83	Asp 9 H^N
Asn 83	0.90	0.31	none
Asn 106	0.90	0.85	Phe 102 O

tion is particularly striking as it is standardly assumed that the solvent exposed side chains are the most likely sites to exhibit substantial conformational/dynamical differences between the crystal and solution structures.

The longer polar and charged side chains exhibit a relatively uniform decrease in order parameters as a function of bonds removed from the main chain. The C^{β} positions of the lysine, arginine, glutamine, and glutamic acid side chains have an average S^2 value of 0.42 with an rmsd of 0.14. With one exception, these side chains have average S^2 values at the C^{γ} position of 0.20 with an rmsd of 0.08. The C^{γ} of Lys 57 is appreciably less mobile (S^2 of 0.47). Both the X-ray and NMR analyses report that the ϵ-amino group of this residue is hydrogen bonded via a water molecule to the buried Asp 26 carboxyl in the active site.

All prolines exhibited S^2 values for $C^{\alpha} > C^{\delta} > C^{\beta} > C^{\gamma}$ consistent with that expected of the two state puckering of the pyrrolidine ring.[58] The proline relaxation parameters are dominated by the S_f^2 factor as anticipated for the ~10−30 ps ring puckering motion.[59] Furthermore the S^2 values at C^{δ}, C^{β}, and C^{γ} of P76 were all approximately 0.2 larger than those for the other prolines as expected for the more rigid cis conformation.[60]

***E. coli* Thioredoxin Dynamics in the Microsecond−Millisecond Range.** Experimental relaxation values lying above the inscribed triangles of Figure 2 exhibit T_1/T_2 values larger than that predicted from the estimated protein tumbling rate. An apparent chemical exchange line broadening can be estimated as the minimal T_2 relaxation contribution required to shift the observed relaxation data down to the triangular boundary. As the experimental data underdetermine the derived dynamical parameters, once again additional justification is warranted to support the assumption of chemical exchange dynamics. Fifty-seven heavy atoms (50 ^{13}C and 7 ^{15}N[42]) exhibit apparent chemical exchange in excess of 1 s^{-1}. Most of these atoms also exhibit large order parameters. This selectivity reflects the fact that in most cases a nucleus having a low order parameter as well as chemical exchange cannot be distinguished from the case of an intermediate order parameter as long as the relaxation values lie within the boundaries shown in Figure 2.

Nearly 80% of these 57 nuclei exhibiting apparent chemical exchange lie within either the active site loop or in the four structural regions illustrated in Figure 5. In contrast for the 19 residues (54 monitored nuclei) between the sites of exchange at T8 and start of the active site loop, only a single case of apparent chemical exchange was observed. This marked spatial clustering is strongly suggestive of collective dynamical processes consistent with conformational transitions in the microsecond−millisecond time frame.

For each of the four regions shown in Figure 5 the nuclei exhibiting apparent chemical exchange line broadening are clustered around sites of side chain-main chain or bifurcated main chain hydrogen bonds which were discussed in detail in the high resolution X-ray structural analysis.[23] Breaking and/or rearrangement of these hydrogen bonds provides a straightforward rationalization for the activation energy barrier needed to produce conformational transitions in the microsecond−millisecond time frame. This interpretation is reinforced by the fact that the nuclei showing the largest line broadening are generally closest to the hydrogen bonding site (e.g., N106 C^{β}, T8 C^{β}, and L42 C^{α}).

By far the most extensive site of chemical exchange (21 of 57) extends through the active site loop from F27 at the end of the β_2 strand to K36 in the beginning of the α_2 helix. In addition, at minimum, the structurally abutting I75 C^{δ} and P76 C^{δ} as well as the buried D26 C^{β} also would appear to be part of this site. It should be noted that the S^2 value of I75 $C^{\gamma 2}$ is twice that of all the other I $C^{\gamma 2}$ positions almost surely indicating chemical exchange. However, since the relaxation data for this nucleus can be fitted exactly by the (S_f^2,S_H^2,S_C^2) formalism, no unambiguous partitioning of chemical exchange contributions is possible.

Given the limitations of the chemical exchange analysis primarily to nuclei that are relatively immobile on the nanosecond time frame, there is a strong correspondence to the set of nuclei exhibiting chemical shift changes induced upon reduction of the active site disulfide.[61] Excluding the aromatic rings (^{13}C chemical shift differences not reported), for residues A29 to K36 N and I75 C^{δ} + P76 C^{δ}, 15 of 16 ^{13}C and ^{15}N

(58) London, R. E. *J. Am. Chem. Soc.* **1978**, *100*, 2678−2685.

(59) Sarkar, S. K.; Young, P. E.; Torchia, D. A. *J. Am. Chem. Soc.* **1986**, *108*, 6459−6464.

(60) Fossel, E. T.; Easwaran, K. R. K.; Blout, E. R. *Biopolymers* **1975**, *14*, 927−935.

(61) Chandrasekhar, K.; Campbell, A. P.; Jeng, M. F.; Holmgren, A.; Dyson, H. J. *J. Biomolec. NMR* **1994**, *4*, 411−432.

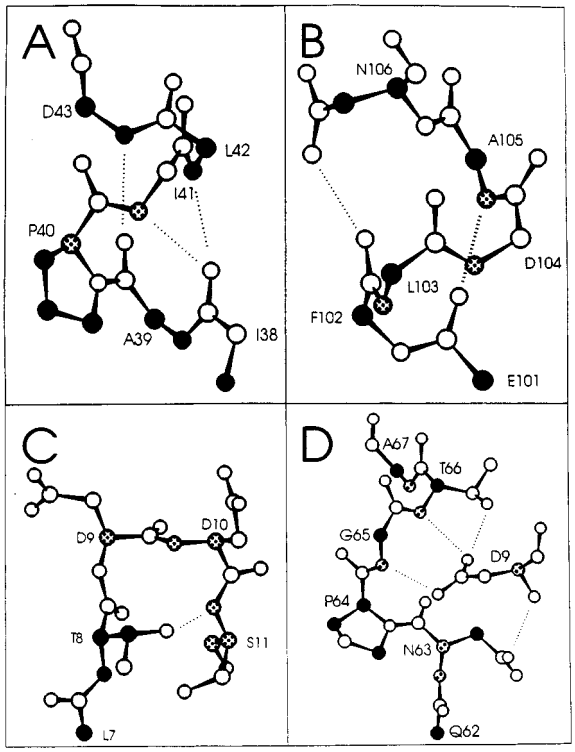

Figure 5. Chemical exchange dynamics centered around side chain-main chain and bifurcated main chain hydrogen bonds in *E. coli* thioredoxin. The X-ray analysis[23] indicated that in the middle of the α_2 helix the carbonyl of I38 hydrogen bonds to the amides of both I41 and L42, presumably due to the presence of the internal P40 residue. In panel A (adapted from Figure 6b[23]) 10 of the 12 monitored main chain and proline nuclei exhibit line broadening (black = observed line broadening, speckled = observed but no apparent line broadening). Residue names are placed adjacent to the α carbons. Panel B (adapted from Figure 6c[23]) illustrates the sites of chemical exchange for nuclei ($S^2 > 0.75$) surrounding the hydrogen bond between side chain amide of N106 and the main chain carbonyl of F102. For the case of the T8 side chain hydrogen bond to the main chain amide of S11 in panel C chemical exchange dynamics are apparent only on the T8 side of the β turn (adapted from Figure 8a[23]). Finally, as discussed in the X-ray analysis, the multiple hydrogen bonding interactions of D9 appear to stabilize the irregular structure lying between the short α_3 helix (residues 59−63) and the 3_{10} helix (residues 66−70). Panel D indicates significant chemical exchange for this region (adapted from Figure 9[23]). It should be noted that in addition to experimental uncertainty, the absence of chemical exchange can arise from similar chemical shift values in both conformations for a given nucleus.

nuclei exhibiting line broadening also exhibit differential chemical shifts. Conversely, excluding E30 C^β and P34 C^γ (both have $S^2 < 0.40$), for the same residues only three nuclei exhibit differential chemical shifts but no line broadening. These three nuclei G33 C^α, P34 C^α, and C35 N are discussed in Figure 6. The active site line broadening can not represent exchange with trace amounts of the reduced state since the rate of the redox transition is far into the slow exchange limit at this low pH (personal observation). Given the modest precision in both the line broadening and differential chemical shifts, the substantial correlation is highly suggestive of a transient reduced-like conformation.

Formation of a transient reduced-like active site conformation in the oxidized state in the microsecond−millisecond time frame requires a corresponding activation barrier for the transition. Disulfide bond conformational transitions between gauche$^+$ and gauche$^-$ can yield chemical exchange broadening in proteins.[51] However, the cysteine sulfurs of the oxidized and reduced forms of *E. coli* thioredoxin retain a similar relative orientation

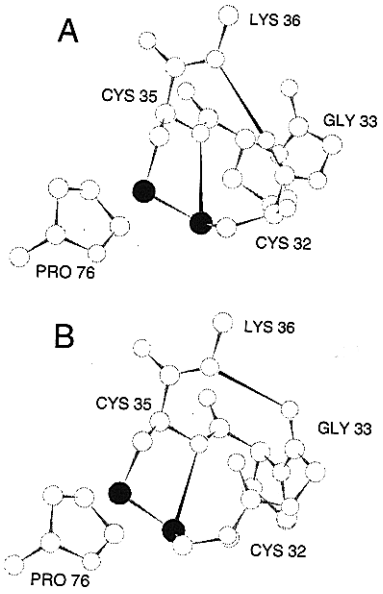

Figure 6. Model for transient active site conformation of oxidized *E. coli* thioredoxin. The active site conformation observed in the X-ray structural model[23] is illustrated in panel A with the cystine sulfurs marked in black. Rigid dihedral angle alterations of this model were carried out to accommodate a change in the hydrogen bonding of K36 NH from the C32 carbonyl to the G33 carbonyl (as was observed upon reduction[63]) while preserving the disulfide linkage as illustrated in panel B. Only the (ϕ,ψ) angles of C35 were altered to the canonical 3_{10} helical values of (−55,−30)[65] since P34 has approximately these dihedral angles in the X-ray structure. The cysteine χ_1 angles were then adjusted so as to reestablish the disulfide bond distance while simultaneously equalizing the C^β−S−S bond angles (6° change for the χ_1 values of both C32 and C35) (to 160° and −70°, respectively). In contrast to the X-ray model conformation in which C35 S^γ is at van der Waals distance from P76 C^α and C^β, this distance shortens 0.4−0.5 Å with the pyrrolidine ring of P76 pressed against the top of the disulfide linkage. Although no constraint was imposed, the distance from C35 N to C32 S^γ in panel B is 3.1 Å with a satisfactory hydrogen bonding orientation. In contrast to the remainder of the active site loop, the main chain positions spanned by both the disulfide linkage and the hydrogen bond between C35 N and C32 S^γ exhibit differential chemical shifts upon reduction but no line broadening in the oxidized state. The main chain X-ray B-factors exhibit a pronounced decrease for these residues relative to those immediately adjacent potentially consistent with the presence of a relative conformational shift at either end of this segment.[23]

suggesting that reduction would not be coupled to such a torsional transition of the disulfide bond.

On the other hand, the analysis of the structural regions illustrated in Figure 5 clearly indicates the utility of hydrogen bond rearrangement for providing a suitable activation barrier. Analysis of the oxidized and reduced structures[62] indicate that in the active site only a single bifurcated main chain hydrogen bond rearrangement is observed. The first hydrogen bond donor of the α_2 helix K36 NH forms hydrogen bonds to the carbonyls of both C32 and G33 in the X-ray structure.[23] The solution structural analysis[63] indicates that upon reduction K36 NH switches from the carbonyl of C32 to that of G33. Furthermore, the structural homologous *E. coli* glutaredoxin undergoes the same tightening of the first turn of the α-helix to the 3_{10} helical form upon reduction of the disulfide.[64] Hence it seems plausible to suggest that this hydrogen bond rearrangement might also

(62) Jeng, M.-F.; Campbell, A. P.; Begley, T.; Holmgren, A.; Case, D. A.; Wright, P. E.; Dyson, H. J. *Structure* **1994**, *2*, 853−868.
(63) Jeng, M. F.; Campbell, A. P.; Begley, T.; Holmgren, A.; Case, D. A.; Wright, P. E.; Dyson, H. J. *Structure* **1994**, *2*, 853−868.
(64) Xia, T. H.; Bushweller, J. H.; Sodano, P.; Billeter, M.; Bjornberg, O.; Holmgren, A.; Wuthrich, K. *Prot. Sci.* **1992**, *1*, 310−321.

occur transiently in the oxidized state giving rise to the observed pattern of line broadening.

In order to examine the physical plausibility of such a hydrogen bond shift under to constraint of the disulfide bond, a simple model building analysis was carried out assuming the minimal structural transition (Figure 6). Starting from the X-ray coordinates, only the (ϕ,ψ) angles of C35 need be altered to the canonical 3_{10} helical values of (−55,−30)[65] since P34 has approximately these dihedral angles in the X-ray structure. Note that the NMR analysis of the structurally homologous human thioredoxin[66] indicates a similar localized change of the C35 dihedral angles upon reduction. The cysteine χ_1 angles were then adjusted so as to reestablish the disulfide bond distance while simultaneously equalizing the $C^{\beta}-S-S$ bond angles. This was achieved by an ∼6° change for the χ_1 values of both C32 and C35 (to 160° and −70°, respectively).

Several features of this model are worthy of note. Although no constraint was imposed, the distance from C35 N to C32 S^{γ} in panel B is 3.1 Å with a satisfactory hydrogen bonding orientation. In the X-ray analysis of the oxidized protein it was observed that this specific interaction would be expected to enhance the susceptibility of C32 S^{γ} to attack. Such electrophilic interactions are known to stabilize the central sulfur of the linear trisulfur transition state.[67] Furthermore, the hydrogen bond between C35 N^{H} and C32 S^{γ} presumably must be preserved in any significantly populated conformation of the oxidized state since reduction, with the attendant disruption of this bond, leads to a 10^4 increase in the amide exchange rate of C35 NH.[68]

Such a conformational transition predicts an increased flexibility of the peptide plane containing K36 H^{N} in order to facilitate a switch from the α helical to the 3_{10} helical hydrogen bonding arrangement in the active site. It should be noted that the ^{15}N relaxation data of the oxidized protein[42] predicts a larger chemical exchange line broadening contribution for Lys 36 H^{N} than for any of the other reported main chain amides in the active site loop or in the structural regions illustrated in Figure 5. The apparent increased mobility of this peptide plane presumably results from the fact that the carbonyl of C35 has no main chain hydrogen bond donor.[23] Instead the carbonyl of K36 is hydrogen bonded to A39 NH (the presumptive α-helical donor for the carbonyl of C35). This breakdown in the standard α-helical hydrogen bonding pattern is due to the presence of P40 in the middle of the α_2 helix which eliminates the normal donor for the carbonyl of K36.

The only apparent steric constraint to the conformational transition modeled in Figure 6B is the compression of the top of the disulfide linkage against the pyrrolidine ring of the cis P76. In the X-ray model conformation (Figure 6A) C35 S^{γ} is at van der Waals distance from P76 C^{α} and C^{β}. In Figure 6B this distance shortens 0.4−0.5 Å potentially forcing a reduction of the $C^{\beta}-S-S$ bond angle around C32 S^{γ}. With regards to the potential functional significance of the enhanced mobility of the K36 H^{N} peptide plane and the positioning of the P76 pyrrolidine ring over the disulfide linkage it should be noted that, in addition to the active site cysteines, P40 and P76 are the only absolutely conserved residues for all thioredoxins throughout the various phyla as well as for mammalian to trypanosomal protein disulfide isomerases.[69]

Discussion

Although generally the interior atoms of the protein exhibit a lower mobility than do the solvent accessible atoms, the degree of burial is not a particularly effective indicator of rigidity. The correlation is far better for the increase in mobility as a function of the number of dihedral angles removed from the backbone. In most cases the steric hindrance of the protein matrix merely reduces the steepness of this gradient of increased mobility. Only a subset of the aromatic residues show a clear violation of this behavior. As indicated from the model analysis of the dynamical parameters of Phe 12, although substantial side chain dihedral angle excursions appear energetically feasible, the steric impediment of the protein matrix imposes correlated motion so as to minimize net displacement of the side chain atoms. In this example the relaxation data was shown to be compatible with aromatic ring displacements of a magnitude consistent with the thermal ellipsoids observed by X-ray diffraction and molecular simulations.

Although the large inflexible aromatic rings serve to render these residues particularly sensitive to the steric constraints of the protein matrix, it can be anticipated that the other buried side chains would show analogous correlated motion on a more attenuated scale. The low rotation axis order parameters of the leucine methyl side chains of staphylococcal nuclease[11] compared to the high order parameters of the corresponding main chain amides[70] have been interpreted as being in conflict with the observed similarity of the crystallographic temperature factors for these methyl carbons and those of the main chain heavy atoms. A substantial complication in the comparison between crystallographic and NMR relaxation data arises from the fact that the B-factor samples the translational disorder of the heavy atom, while the relaxation monitors the orientational disorder of the H−C vector. Hence any comparison necessitates a molecular modeling of the underlying motion.

Simulations of correlated main chain-side chain torsion angle oscillations of the thioredoxin leucine residues analogous to those carried out for the phenylalanine side chains indicate that a contradiction with the crystallographic results need not be present. The most mobile leucine side chain in *E. coli* thioredoxin Leu 58 has an S^2 of 0.90 at C_{α} and an average methyl S_{axis}^2 of 0.39 which according to the uniform restricted diffusion model yields maximal angles of +/−20° and 62°, respectively. For side chain conformational transitions consistent with these order parameters the average shift in coordinates of C^{γ} and the two C^{δ} atoms can be minimized to 0.56 Å with correlated oscillations of 20°, 22°, and 36° for ϕ, χ_1, and χ_2, respectively. This angle triplet is by no means an isolated solution as χ_1 values ranging from 12° to 28° and χ_2 values ranging from 33° to 42° predict average coordinate shift values for the C^{γ} and C^{δ} carbons within 10%.

As the predicted S_{axis}^2 values along the two $C^{\gamma}-C^{\delta}$ vectors can readily differ by 0.1, the local anisotropy of such correlated main chain-side chain torsional oscillations may provide an explanation for the nonequivalence of geminal S_{axis}^2 values previously noted.[11,38,41] More generally these calculations suggest that even for buried side chains, low order parameters at the distal carbons need not be indicative of transitions between rotamer minima.

The chemical exchange data of *E. coli* thioredoxin strongly suggests that hydrogen bond rearrangements may routinely serve as the primary activation energy barrier for conformational transitions in the microsecond−millisecond timeframe. Such dynamical switches are of potential functional interest as this

(65) Prasad, B. V. V.; Sasisekharan, V. *Macromolecules* **1979**, *12*, 1107−1110.
(66) Qin, J.; Clore, G. M.; Gronenborn, A. M. *Structure* **1994**, *2*, 503−522.
(67) Pappas, J. A. *J. Am. Chem. Soc.* **1977**, *99*, 2926−2930.
(68) Jeng, M.-F.; Dyson, H. J. *Biochemistry* **1995**, *34*, 611−619.
(69) Eklund, H.; Gleason, F. K.; Holmgren, A. *Proteins* **1991**, *11*, 13−28.
(70) Kay, L. E.; Torchia, D. A.; Bax, A. *Biochemistry* **1989**, *28*, 8972−8979.

is the timeframe characteristic of a wide range of enzymatic turnover rates and allosteric transitions. Although the enzymatic turnover rate has not been determined for *E. coli* thioredoxin, the reduction of the oxidized protein by dithiothreitol is linear to at least 10 mM with a second order rate constant of 1600 s^{-1} M^{-1} at pH 7.2.[71] In contrast, at neutral pH dithiothreitol reduces neutral small molecule acyclic disulfides 5000-fold more slowly.[72]

The X-ray analysis[23] proposed that the positioning of the disulfide spanning directly over the N-terminus of the α_2 helix could serve to stabilize the anionic linear trisulfur S_N2 transition state formed in the reduction reaction. Furthermore, as mentioned above, the direct Cys 35 H^N hydrogen bond to the Cys 32 sulfur should facilitate the nucleophilic attack on that site.[67] On the other hand, the high resolution X-ray structure found no evidence of strained dihedral or bond angles at the disulfide. Five membered cyclic disulfides are well known to exhibit ~600 fold enhanced reactivity due to the ring strain effects.[73] Given the extreme reactivity of the thioredoxin disulfide, additional mechanisms may fruitfully be considered.

The active site conformational transition modeled in Figure 6 indicates an involvement of the two absolutely conserved residues Pro 40 and Pro 76 for which no clear functional role has yet been proposed. As suggested, the absence of an α helical hydrogen bond donor at residue 40 may allow increased flexibility of the peptide plane of Lys 36 H^N thus facilitating its shift from the carbonyl of Cys 32 to that of Gly 33. This model transition indicates that the tightening of the helical axis would force the Cys 35 sulfur into the pyrrolidine ring potentially compressing the Cys 32 C^{β}-S-S bond angle toward the transition state value of 90°. In analogy to the known ring strain effects on the reactivity of five membered cyclic disulfides the resultant stabilization of the linear trisulfur transition state could substantially enhance the rate of reduction.

If such a bond angle compression mechanism is utilized to enhance the reactivity of the thioredoxin disulfide, one needs consider the potential justification of a transient conformational distortion. If instead the disulfide was statically strained, energetic compensation would be required for this localized strain. The resultant alteration of the relative thermodynamical stability of the oxidized and reduced states of the protein directly affects its redox potential.[74] The redox potential of −270 mV[75] appears well matched to the cellular environment of *E. coli* since thioredoxin is half reduced in vivo.[76] On the other hand, if the oxidized protein transiently samples the strained disulfide conformation at a rate consistent with the enzymatic turnover number, the kinetic benefit of the strained disulfide can be achieved at a modest thermodynamic cost.

Acknowledgment. This work was supported by National Institutes of Health grant GM 38779 and by National Science Foundation Grant DMB-8957336. We would like to thank F. M. Richards for providing his ACCESS program for the calculation of static solvent accessibility. Support from the W. M. Keck Foundation for the initial phases of this work is gratefully acknowledged. ^{13}C relaxation data will be deposited at the Biological Magnetic Resonance Bank and the ^{13}C labeling strain DL323 at the Coli Genetic Stock Center following publication.

JA960877R

(71) Holmgren, A. *J. Biol. Chem.* **1979**, *254*, 9627−9632.
(72) Creighton, T. E. *J. Mol. Biol.* **1975**, *96*, 767−776.
(73) Singh, R.; Whitesides, G. M. *J. Am. Chem. Soc.* **1990**, *112*, 6304−6309.
(74) Lin, T.-Y.; Kim, P. S. *Biochemistry* **1989**, *28*, 5282−5287.
(75) Krause, G.; Lundstrom, J.; Lopez-Barea, J.; Cuesta, C. P. d. l.; Holmgren, A. *J. Biol. Chem.* **1991**, *266*, 9494−9500.
(76) Fagerstadt, M.; Holmgren, A. *J. Biol. Chem.* **1982**, *257*, 6926−6930.
(77) LeMaster, D. M.; Cronan, J. E. *J. Biol. Chem.* **1982**, *257*, 1224−1230.
(78) LeMaster, D. M.; Richards, F. M. *Anal. Bioch.* **1982**, *122*, 238−247.